IMPLEMENTATION OF A CREEP MODEL IN FLAC TO STUDY THE THERMOMECHANICAL RESPONSE OF SALT AS A HOST REPOSITORY MEDIUM— 2ND PROGRESS REPORT

Prepared for

U.S. Nuclear Regulatory Commission
Contract No. NRC–HQ–12–C–02–0089

Prepared by

Goodluck Ofoegbu
Biswajit Dasgupta

Center for Nuclear Waste Regulatory Analyses
San Antonio, Texas

March 2017

CONTENTS

CONTENTS (Continued)

FIGURES

TABLE

ACKNOWLEDGMENTS

This report was prepared to document work performed by the Center for Nuclear Waste Regulatory Analyses (CNWRA®) for the U.S. Nuclear Regulatory Commission (NRC) under Contract No. NRC–HQ–12–C–02–0089. The activities reported here were performed on behalf of the NRC Office of Nuclear Material Safety and Safeguards, Division of Spent Fuel Management. The report is an independent product of CNWRA and does not necessarily reflect the view or regulatory position of NRC. The authors gratefully acknowledge the technical and editorial reviews of David Pickett and the programmatic review of Gordon Wittmeyer, and the assistance of Arturo Ramos in preparing this report.

QUALITY OF DATA, ANALYSES, AND CODE DEVELOPMENT

DATA: All CNWRA-generated original data contained in this report meet the quality assurance requirements described in the Center for Nuclear Waste Regulatory Analyses Quality Assurance Manual.

ANALYSES AND CODES: The computer software code FLAC® Versions 7.0 (Itasca Consulting Group, 2011) and 8.0 (Itasca Consulting Group, 2016) was used in the analyses contained in this report. FLAC is commercial software controlled under Technical Operating Procedure (TOP)–018, Development and Control of Scientific and Engineering Software. Documentation of the calculations can be found in Scientific Notebook 1237E (Dasgupta and Ofoegbu, 2017).

REFERENCES

Dasgupta, B. and G. Ofoegbu. "Numerical Implementation, Testing, and Use of a Constitutive Model for Mechanical Behavior of Salt." Scientific Notebook No. 1237E. San Antonio, Texas: Center for Nuclear Waste Regulatory Analyses. 2017.

Itasca Consulting Group, Inc. "FLAC Fast Lagrangian Analysis of Continua." Version 8. Minneapolis, Minnesota: Itasca Consulting Group, Inc. 2016.

_____. "FLAC Fast Lagrangian Analysis of Continua." Version 7. Minneapolis, Minnesota: Itasca Consulting Group, Inc. 2011.

1 INTRODUCTION

1.1 Background

This project continues studies conducted on behalf of the U.S. Nuclear Regulatory Commission (NRC) to assess the mechanical behavior of salt rock in the generic context of geologic disposal of high-level radioactive waste. In a previous study, Ofoegbu and Dasgupta (2016) developed a computer code module in FLAC (Fast Lagrangian Analysis of Continua; Itasca Consulting Group, 2011) to implement a European Commission salt model known as FZK-INE (European Commission, 2007) and used the implementation to model two in-situ experiments on time-dependent deformation of underground openings in salt rock conducted previously at the Waste Isolation Pilot Plant (WIPP).

To determine values of mechanical parameters for the modeling, Ofoegbu and Dasgupta (2016) used the FLAC implementation of the FZK-INE model to simulate triaxial compression creep testing to match actual laboratory test results of WIPP salt from Mellegard and Munson (1997). The simulated testing showed that the strain versus time behavior of the salt is represented adequately by the transient creep function alone, among the three potential creep strain contributions included in the FZK-INE model—transient creep, steady-state creep, and damage creep. Therefore, the analysis focused on evaluating the three transient creep parameters a_0, a_1, and a_2, as described in Ofoegbu and Dasgupta (2016, Chapter 3).

As discussed in Ofoegbu and Dasgupta (2016), modeling time-dependent deformation of Rooms B and D of the WIPP tests using the creep model as discussed in the foregoing paragraph indicates the simulated underground openings stabilize after approximately 300 days. In contrast, the field test data show the openings continued to converge through the test duration of approximately 1,500 days. The amount of convergence predicted using the model is much smaller than the measured convergence.

1.2 Representation of Small Deviatoric Stress in Creep Analysis

A recent study conducted under an international (United States and Germany) collaborative project (Reedlunn, 2016) reached a similar conclusion: convergence calculated using creep models is only about one third of the measured convergence. Reedlunn (2016) also observed that most of the difference between the calculated and measured convergence occurs during the first 50 days following excavation of the WIPP openings. The study identified seven potential technical gaps that could contribute to the difference. Four of the technical gaps raise questions regarding material modeling of the salt rock, whereas three relate to geologic characterization.

The following technical gaps raise questions regarding material modeling of salt rock and geometrical modeling of the underground excavations.

1. **Creep of salt at small deviatoric stress**. Available data indicate that calculated creep rates at deviatoric stress smaller than approximately 10 MPa[1] are orders of magnitude smaller than creep rates derived based on laboratory and field data for similar stress conditions. This difference could result in creep models underpredicting potential convergence. Although the strain rate for such stress conditions is small, the overall

[1] 1.0 MPa = 145.03 psi

contribution to convergence could be large because the volume of rock subjected to such stress conditions is usually larger than the volume subjected to greater stress.

2. **Sliding at clay seams**. Contributions of clay seam deformation to convergence of the openings is affected by the material and geometrical models used to represent the clay seams. The strength and stiffness properties of clay seams, however, may not be well characterized.

3. **Strength of anhydrite layers within the salt rock**. This question could be important but needs to be applied to the entire rock body, not just the anhydrite layers. The strength of rock determines the occurrence of stress-driven time-independent inelastic deformation and could affect the magnitudes of calculated deformation such as convergence of an underground opening.

4. **Extent of geometrical model around simulated underground openings**. The geometrical model extent could be an issue because of potential contributions of zones of small deviatoric stress. The fraction of the geometrical model subjected to small deviatoric stress increases as the model extent increases.

1.3 Current Report

Ofoegbu and Dasgupta (2016) attributed the difference between the calculated and measured convergence to Items 2 and 3 in Section 1.2 (i.e., representation of the clay seams and strength of salt rock in the numerical model). The report identified contributions due to potential inelastic deformation mechanisms other than creep to explain the difference between the calculated and measured convergence. The measured convergence compared with the calculated results suggested that inelastic deformation mechanisms other than creep likely occurred in the field test. However, the calculation was performed using a material model that included only creep as the mechanism for inelastic deformation. The analysis in Ofoegbu and Dasgupta (2016) included modifying the creep parameters to increase the rate of modeled creep deformation, but the results indicated that the creep rate could not be increased enough to obtain convergence histories similar to the field measurements. In order to calculate convergence histories similar to the measurement, the model needed to be modified to include deformation due to material failure in addition to creep.

1.3.1 Inelastic Deformation Related to Strength of Salt Rock

We discuss a model of the strength of salt rock in order to develop a procedure for calculating potential inelastic deformations due to stress conditions that overcome the rock strength. Such deformations are time-independent and occur in addition to creep deformations. As Ofoegbu and Dasgupta (2016) discuss, several deformation mechanisms could contribute strain increments, such as Δe_{ij}^{E}, Δe_{ij}^{P}, Δe_{ij}^{Th}, Δe_{ij}^{D}, and Δe_{ij}^{C}, due to elastic, plastic, thermal-expansion, damage, and creep deformation mechanisms, respectively. The stress-strain relationships for the material are based on the assumption that the strain contributions of the various deformation mechanisms are separable and additive. The assumption is based on common practice and is fundamental to modeling generalized stress-strain relationships (e.g., Desai and Siriwardane, 1984; p. 223). The assumption of separability implies that each strain contribution can be modeled separately based on an understanding of the associated deformation mechanism. The assumption of additivity implies the various strain contributions can be added to obtain the total strain increment.

Ofoegbu and Dasgupta (2016) describe the implementation and testing of a creep model (model for Δe_{ij}^{C}). In addition, the overall incremental stress-strain model and the models for creep strain and thermal strain (Δe_{ij}^{Th}) were described in Ofoegbu and Dasgupta (2016) and are repeated in Chapter 2 of this report. In Chapter 3, we describe the development and implementation of a plastic deformation model (model for $\Delta e_{ij}^{P} + \Delta e_{ij}^{D}$) to account for potential inelastic strain contributions due to material failure (i.e., deformation driven by stress conditions that overcome the material strength). The resulting material model, which includes all strain contributions in Eq. (2-2), is used to model the WIPP Rooms B and D field tests. The numerical modeling is discussed in Chapter 4.

1.3.2 Creep Modeling for Conditions of Small Deviatoric Stress

Reedlunn (2016, Figures 3.7b and 3.8b) compared model calculations against laboratory data to show that current creep modeling under-predicts creep of salt for deviatoric stress smaller than approximately 10 MPa. The data indicate the creep strain relationship with deviatoric stress changes at a deviatoric stress of approximately 10 MPa and suggest that the approach to creep modeling may need to be modified to account for stress dependence of creep strain rate versus stress relationships. We approach the problem in the current study by describing a key creep parameter as a function of deviatoric stress. We introduced the concept of a stress-dependent creep parameter in the earlier study (Ofoegbu and Dasgupta, 2016, Figure 3-8) but modify the relationship in this study to better represent the laboratory data discussed in Chapter 2 (Section 2.1). We describe an analysis case in Chapter 4 to examine the effect of the modification.

2 INCREMENTAL STRESS-STRAIN MODEL FOR SALT ROCK

As discussed in Section 1.3.1, the total strain increment is represented as a sum of several contributions, as follows:

$$\Delta e_{ij} = \Delta e_{ij}^{E} + \Delta e_{ij}^{P} + \Delta e_{ij}^{Th} + \Delta e_{ij}^{D} + \Delta e_{ij}^{C} \tag{2-1}$$

This equation implies the elastic strain increment can be expressed in terms of the other strain contributions, as follows:

$$\Delta e_{ij}^{E} = \Delta e_{ij} - \Delta e_{ij}^{P} - \Delta e_{ij}^{Th} - \Delta e_{ij}^{D} - \Delta e_{ij}^{C} \tag{2-2}$$

The elastic stress-strain relationship for the material can be expressed in terms of Hooke's law and Eq. (2-2) provides a way to incorporate the other strain contributions into the relationship, resulting in the following:

$$\Delta\sigma_{ij} = C_{ijkl}\Delta e_{kl}^{E} = C_{ijkl}\left(\Delta e_{kl} - \Delta e_{kl}^{P} - \Delta e_{kl}^{Th} - \Delta e_{kl}^{D} - \Delta e_{kl}^{C}\right) \tag{2-3}$$

where C_{ijkl} is the elastic stiffness tensor, defined as follows for an isotropic material,

$$C_{ijkl} = \lambda\delta_{ij}\delta_{kl} + 2G\delta_{ik}\delta_{jl} \tag{2-4}$$

with shear modulus, G, and Lame parameter, λ, related to the bulk modulus, K, and Poisson's ratio, ν, as shown in Eq. (2-5); and δ_{ij} is the Kronecker delta ($\delta_{ij} = 1$ if $i = j$ and $\delta_{ij} = 0$ if $i \neq j$).

$$\lambda = 3K\nu/(1+\nu)\,; \qquad G = (3/2)(K - \lambda) \tag{2-5}$$

In an initial implementation of the constitutive model, described in Ofoegbu and Dasgupta (2016), the authors assumed creep was the dominant deformation mechanism. Instantaneous rock material failure, which we model using plasticity theory as described in Chapter 3, was not included in the initial implementation. We reproduce the description of the initial implementation in this chapter because the implementation provides equations used as part of the more complete implementation described in Chapter 3. For the implementation described in this chapter, plastic deformation is not included, therefore, the plastic strain increment, $\Delta e_{ij,}^{P}$ is set to zero. Chapter 3 describes an implementation that includes plastic deformation.

The thermal strain increment, Δe_{ij}^{Th}, is related to the temperature increment, ΔT, and thermal expansivity (thermally induced volumetric strain per unit temperature increment) α as follows.

$$\Delta e_{ij}^{Th} = (1/3)\alpha\delta_{ij}\Delta T \tag{2-6}$$

In the FZK-INE material model (European Commission, 2007), the creep strain, Δe_{ij}^{C}, consists of three parts: (i) transient creep, Δe_{ij}^{Ctr}; (ii) steady state creep, Δe_{ij}^{Cs}; and (iii) dilatant (or damage) creep, Δe_{ij}^{Cd}. That is,

$$\Delta e_{ij}^{C} = \Delta e_{ij}^{Ctr} + \Delta e_{ij}^{Cs} + \Delta e_{ij}^{Cd} \tag{2-7}$$

The model, therefore, implies representing damage and healing as creep processes. Although there are possibly better options for representing damage and healing, we implement the FZK-INE model as described in Eq. (2-7) and consider necessary modifications later.
The incremental creep strain contributions are defined as follows based on European Commission (2007).

$$\Delta\epsilon^{Ctr} = a_0(\Delta t)\sigma_{\text{eff}}^{n_t}\exp(-Q/RT)\left[1 + a_1 t^{(a_2-1)}\right] \tag{2-8}$$

$$\Delta\epsilon^{Ctr} = \sqrt{(3/2)\left(\Delta e_{ij}^{Ctr}\right)\left(\Delta e_{ij}^{Ctr}\right)} \tag{2-9}$$

$$\Delta e_{ij}^{Cs} = A(\Delta t)\exp(-Q/RT)(F^s)^{n_s}\frac{\partial F^s}{\partial \sigma_{ij}} \tag{2-10}$$

$$\Delta e_{ij}^{Cd} = A(\Delta t)\exp(-Q/RT)\left(F^d\right)^{n_d}\frac{\partial F^d}{\partial \sigma_{ij}} \tag{2-11}$$

where $\Delta\epsilon^{Ctr}$ is the norm of the transient creep strain increment, related to the tensor components, as defined in Eq. (2-9). The parameters in Eqs. (2-8)–(2-11) are as follows:

A	Structural factor ($A = 2.0\,85 \times 10^{-6}$ MPa^{-5}/s)
Q	Activation energy ($Q = 54.21$ kJ/mol)
R	Universal gas constant [$R = 8.314 \times 10^{-3}$ kJ/(mol·K)]
n_s	Exponent for steady state creep ($n_s = 5$)
n_t	Exponent for transient creep ($n_t = 5$)
n_d	Exponent for dilatant creep ($n_d = 2$: this is a modification from the original reference)
T	Absolute temperature (K)
F^s	Flux function for steady state creep
F^d	Flux function for dilatant creep
t	Time (s)
a_0, a_1, a_2	Transient creep parameters

The flux functions are defined as follows:

$$F^s = \sqrt{J_2} = \sqrt{(1/2)S_{ij}S_{ij}} \tag{2-12}$$

$$S_{ij} = \sigma_{ij} - (1/3)\delta_{ij}\sigma_{kk} \tag{2-13}$$

$$\sigma_{\text{eff}} = \left(\sqrt{3}\right)F^s \tag{2-14}$$

$$F^d = n_2 q^2 - n_1 p^2 \tag{2-15}$$

$$p = -(1/3)\sigma_{kk} \tag{2-16}$$

$$q = \sqrt{3J_2} = \left(\sqrt{3}\right)F^s = \sigma_{\text{eff}} \tag{2-17}$$

$$n_1 = c_1\left[(q/p)^2 - c_2\frac{\eta_0 + \varepsilon_{\text{vol}}}{1 + \varepsilon_{\text{vol}}}\right] \tag{2-18}$$

$$n_2 = 1 - c_3 n_1 (p/q)^2 \tag{2-19}$$

c_1, c_2, c_3 Material parameters for dilatant creep
η_0 Porosity of salt rock in strain-free state, $\eta_0 = 0.0002$
ε_{vol} Cumulative volumetric strain, $\varepsilon_{\text{vol}} = e_{kk}$

It should be noted that q as defined in Eq. (2-17) is 1.5 times the value as defined in European Commission (2007). The definition used here is consistent with standard literature but will affect the values of c_1 and c_3. Also, the sign of $n_1 p^2$ in Eq. (2-15) has been modified from European Commission (2007) and the parameters n_1 and n_2 are treated as independent of p and q in developing expressions for the derivatives of F^d with respect to σ_{ij}. Furthermore, although European Commission (2007) gives $n_d = n_s = 5$, dimensional analysis of Eq. (2-11) shows that the dimension of A requires $n_d = 2$. In addition, evaluation of Eq. (2-11) using parameter values from European Commission (2007) shows that setting $n_d = 5$ results in erratic behavior for the equation, whereas $n_d = 2$ results in a smooth and predictable dilation response. However, in this report the damage strain increment Δe_{ij}^{Cd} was not used; instead, a plasticity deformation model was developed to account for inelastic strain from material failure (Chapter 3).

2.1 Modeling Transient Creep Parameter a_0 as a Function of Deviatoric Stress

Ofoegbu and Dasgupta (2016, Figure 3-8) introduced modeling the transient creep parameter a_0 as stress-dependent. The model relationship has been modified to better represent the data and support a first attempt at accounting for increased creep strain rates for conditions of small deviatoric stress. As discussed in Section 1.3.2, information provided by Reedlunn (2016) indicates that current creep laws underestimate creep strain rates at small deviatoric stress. The a_0 versus q/p model described here supports an attempt to account for increased creep rates at small deviatoric stress, as discussed in Chapter 4.

Parameter a_0 is modeled as follows.

$$a_0 = a_0(R_s) \quad \text{with } R_s = q/p \tag{2-20}$$

2.1.1 Small Deviatoric Stress Condition ($R_s < R_{s1}$)

$$a_0 = a_{01} + \frac{c_1(R_{s1} - R_s)}{1 - c_2(R_{s1} - R_s)} \tag{2-21}$$

$$c_1 = \frac{(1 - c_2 R_{s1})(a_{00} - a_{01})}{R_{s1}} \tag{2-22}$$

2.1.2 Larger Deviatoric Stress Model ($R_s \geq R_{s1}$)

$$a_0 = a_{01} + \frac{R_s - R_{s1}}{b_1 + b_2(R_s - R_{s1})} \tag{2-23}$$

$$b_2 = \frac{R_{s2} - R_{s1} - b_1(a_{02} - a_{01})}{(a_{02} - a_{01})(R_{s2} - R_{s1})} \tag{2-24}$$

The parameter values are as follows.

$a_{00} = 0.1$	Value of a_0 for $R_s = 0$
$a_{01} = 0.004$	Value of a_0 at $R_s = R_{s1}$
$a_{02} = 0.01$	Value of a_0 at $R_s = R_{s2}$
$R_{s1} = 0.5$	Value of R_s at which the models for small deviatoric stress and larger deviatoric stress give the same value for a_0
$R_{s2} = 6.0$	Value of R_s at arbitrary point on the larger deviatoric stress model
$c_2 = 1.5$	Fitting parameter for small deviatoric stress model
$b_1 = 100$	Fitting parameter for larger deviatoric stress model

The a_0 versus R_s relationships are plotted in Figure 2-1 along with supporting data from Ofoegbu and Dasgupta (2016, Figure 3-8).

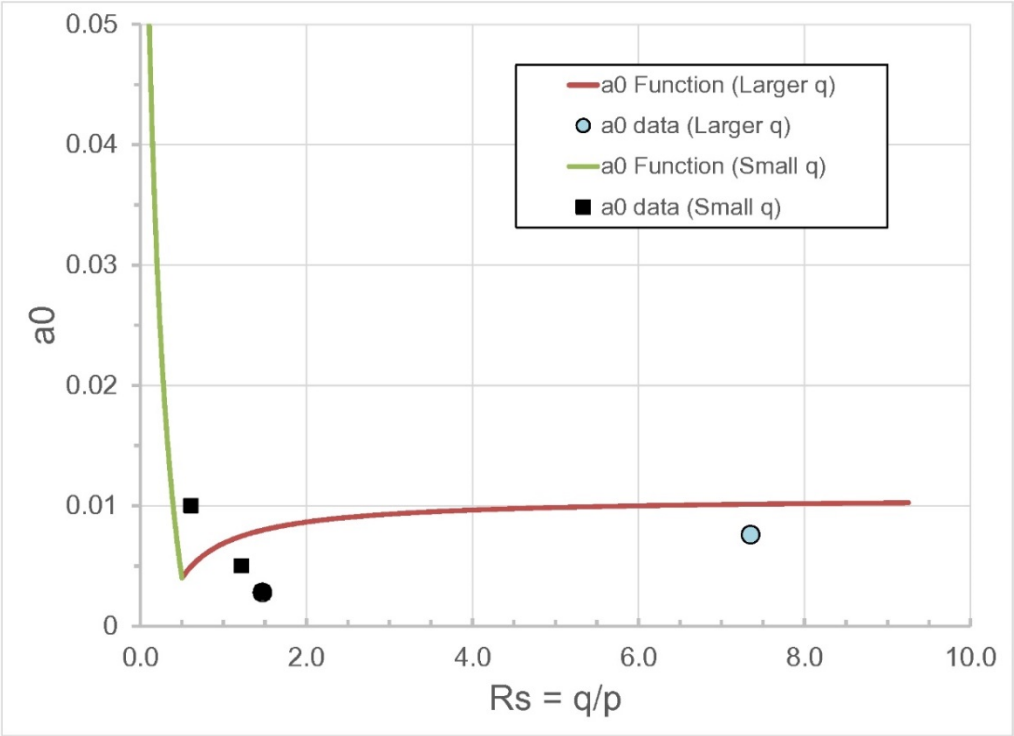

Figure 2-1. Model a_0 Versus R_s Relationships and Data From Ofoegbu and Dasgupta (2016)

3 PLASTICITY MODEL

The plasticity model is based on a generalization of laboratory data to define the stress conditions for time-independent yielding and dilatational behavior of salt rock and compaction of crushed salt. The generalization is based on Hunsche and Hampel (1999) data.

3.1 Material Failure Models for Salt Rock and Crushed Salt

Data reported by Hunsche and Hampel (1999) define a boundary between stress domains for dilation and domains for compaction. We use the data as the basis for developing yield functions and plastic potentials for salt rock and crushed salt. The functions are expressed in terms of q-p relationships, where p is the confining pressure and q is the distortional stress intensity, defined in Eqs. (2-16) and (2-17). The data describe stress conditions in terms of the octahedral shear stress (proportional to q) and mean compressive stress (same as p). Therefore, q-p relationships can be derived based on the data to describe the yield and flow behaviors of the materials.

3.1.1 Yield Function for Salt Rock

Yielding and plastic flow of salt rock are modeled as occurring in stress conditions defined by the domain between the "dilatancy" boundary and the maximum curve of Hunsche and Hampel (1999). The q-p relationships for the domain can be described in terms of a family of curves represented by the following equation.

$$F(p,q) = q - q_0 - \frac{p}{b_1 + b_2 p} = 0 \tag{3-1}$$

Parameters q_0 and b_1 represent the shear resistance of the material, with q_0 representing the cohesive strength and b_1 the frictional strength. Parameter b_2 controls the curvature of the yield surface.

Each yield surface represents a set of values of q_0, b_1, and b_2 (Figure 3-1). The yield surface plot intersects the q axis at $q = q_0$, has an initial slope equal to $1/b_1$ (at $p = 0$), and approaches an asymptote parallel to the p axis at $q = q_0 + 1/b_2$. The top yield surface (i.e., curve with $b_1 = 0.75$ and $b_2 = 0.015$ in Figure 3-1) represents the initial yield condition. Prior to initial yielding, stress states below the top yield surface represent elastic conditions (i.e., no plastic deformation). When the stress state reaches the initial yield surface, plastic deformation occurs, the material weakens as a result, and the yield surface migrates downward (represented by increasing values for b_1 and b_2) as shown by the curves in Figure 3-1.

Downward migration of the yield surface is defined through a relationship between plastic deformation and the strength parameter b_1 (and, by implication, b_2), as we examine subsequently. The yield surface can migrate to as low as the dilation boundary (i.e., curve with $b_1 = 2.0$ and $b_2 = 0.090$ in Figure 3-1), which represents the lowest yield surface in the dilation zone.

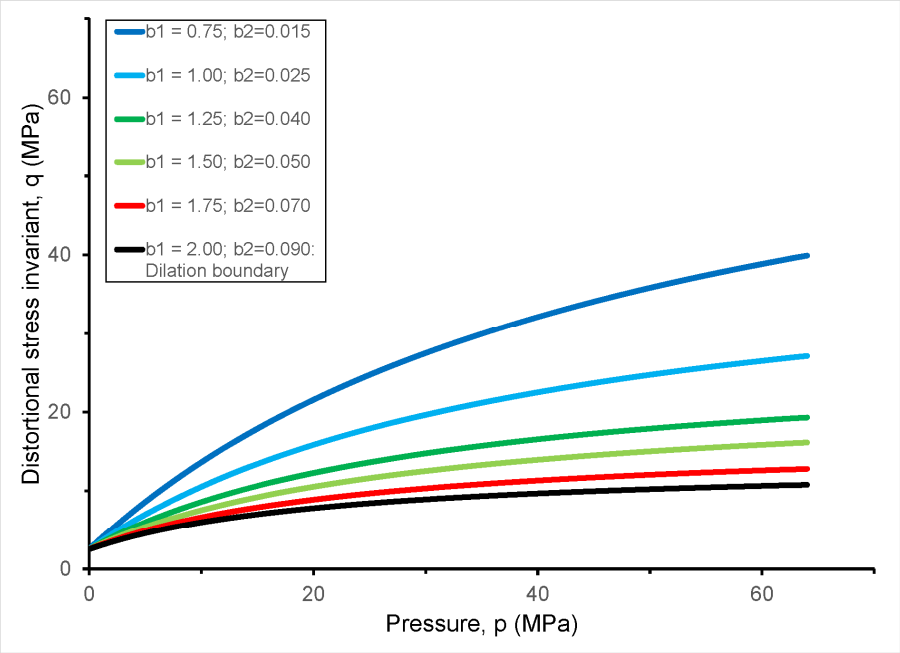

Figure 3-1. Typical Plot of Yield Functions for Salt Rock Based on Eq. (3-1) Using Data From Hunsche and Hampel (1999) ($q_0 = 2.5$ MPa and Values of b_1 and b_2 Shown in the Plot)

3.1.2 Weakening of Salt Rock Due to Inelastic Deformation

Plastic deformation in the dilation zone is accompanied by dilation due to cracking and other deformation mechanisms that cause a nonrecoverable increase in volume. The material weakens as a result. Also, creep deformation may result in loss/rearrangement of particle contacts and strength reduction. Therefore, both creep and plastic deformations could contribute to weakening of the granular network. The weakening is modeled by describing the frictional parameter $b_1$as a function of inelastic strain. Parameter b_2 also varies with inelastic strain but is not independent of b_1. Values of b_1 and b_2 from Figure 3-1 define an approximately linear relationship between the two parameters, as shown in Figure 3-2.

The relationship illustrated in Figure 3-2 is described in the model using Eq. (3-2)

$$b_2 = 0.059 b_1 - 0.033 \tag{3-2}$$

To describe weakening of salt rock due to inelastic deformation, we define a measure of inelastic strain that increases monotonically as plastic, creep, or both plastic and creep deformations occur. The inelastic strain measure represents inelastic distortion, increases whenever plastic or creep deformation occurs, and is denoted Γ^N (inelastic distortional strain), with contributions Γ^P (plastic distortional strain) and Γ^C (creep distortional strain). The plastic contribution is defined as follows.

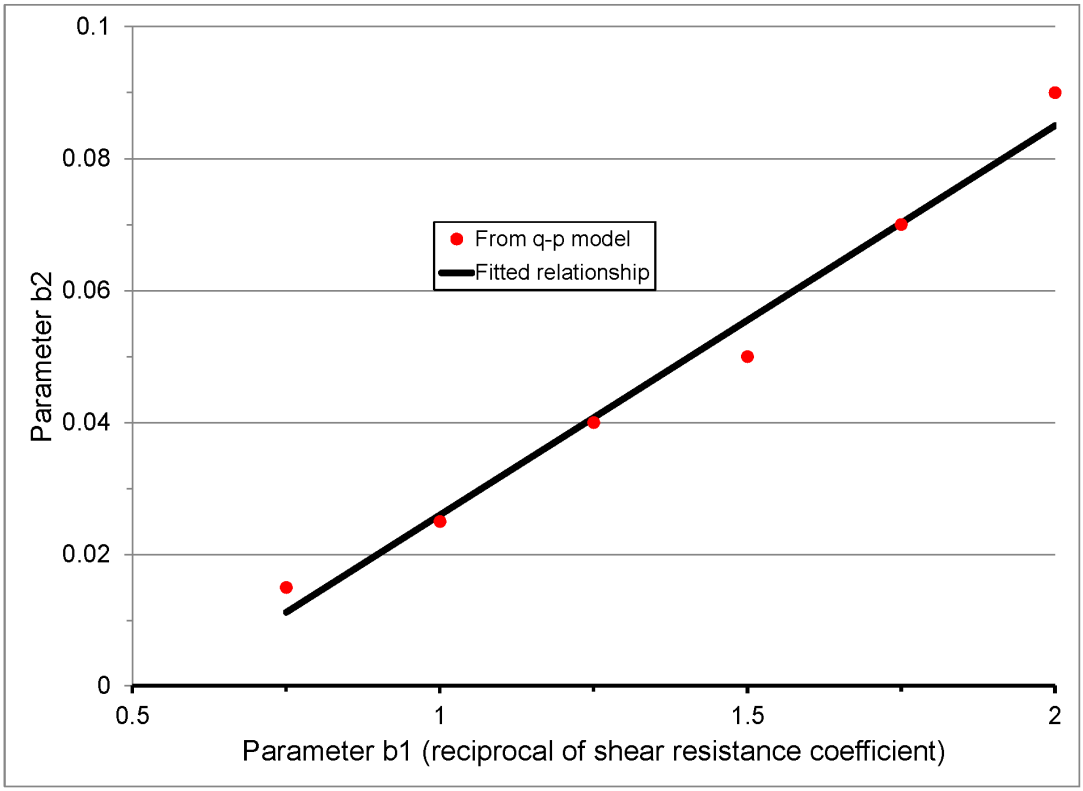

Figure 3-2. Parameter b_2 Described as a Function of Frictional Parameter b_1 Based on Figure 3-1

$$\Gamma^P = \int_0^t \Delta\Gamma^P \tag{3-3}$$

$$\Delta\Gamma^P = \sqrt{\frac{1}{2}\Delta\tilde{e}_{ij}^P \Delta\tilde{e}_{ij}^P} \tag{3-4}$$

$$\Delta\tilde{e}_{ij}^P = \Delta e_{ij}^P - \frac{1}{3}\Delta e_{kk}^P \delta_{ij} \tag{3-5}$$

where $\Delta\tilde{e}_{ij}^P$ represents the deviatoric components of the plastic strain increment tensor. The creep strain contribution Γ^C is also defined as in Eqs. (3-3)–(3-5) with creep strain replacing

plastic strain in the equations. Then, the inelastic distortional strain is obtained as the sum of the plastic and creep contributions as follows.

$$\Gamma^N = \Gamma^P + \Gamma^C \tag{3-6}$$

To define the relationship of b_1 with plastic strain, let $\mu = 1/b_1$ represent the gradient of the yield surface at $p = 0$. Parameter μ is referred to hereafter as the "shear resistance coefficient," representing the frictional strength, and is proportional to the material coefficient of friction. The parameter has a maximum value $\mu_{\max}$ that represents the initial (maximum strength) yield surface and a minimum value $\mu_{\min}$ that represents the dilation boundary (minimum strength yield surface). The material weakening function defines the decay of μ from $\mu_{\max}$ to $\mu_{\min}$ as a function of Γ^P. We will model the decay using a hyperbolic secant function, as follows.

$$\mu = \mu_{\min} + \frac{2(\mu_{max} - \mu_{min})}{\exp(d_c\Gamma^N) + \exp(-d_c\Gamma^N)} \tag{3-7}$$

where d_c is the decay parameter.

Plots of the shear resistance function $\mu(\Gamma^N)$ are shown in Figure 3-3 for $\mu_{\min} = 0.5$, $\mu_{\max} = 1.33$, and selected values of d_c. As Figure 3-3 illustrates, the value of d_c has an important effect on the function. Shear resistance reaches a minimum value at an inelastic distortional strain of 10 percent with $d_c = 50$. For $d_c = 25$, the shear resistance reaches a minimum value at an inelastic distortional strain of 20 percent.

3.1.3 Parameters for Salt Rock Plasticity Model

Based on Eqs. (3-1), (3-2), and (3-7), four parameters are needed to define the salt rock plasticity model: (i) the cohesive strength parameter q_0 and (ii) frictional strength parameters $\mu_{\max}$, $\mu_{\min}$, and d_c. These parameters are needed in addition to the creep strain parameters because of the coupling of plastic and creep deformations through Eqs. (3-6) and (3-7). We obtain a starting guess of $q_0 = 2.5$ MPa, $\mu_{\min} = 0.5$, $\mu_{\max} = 1.33$, and $d_c = 10$ based on the discussion in Sections 3.1.1 and 3.1.2. These values will be modified as necessary based on trial model calculations for the WIPP Room D experiment.

3.2 Plastic Strain-Stress Relationships for Salt Rock

Plastic strain-stress relationships are needed to define the plastic strain increment as a function of stress and deformation history. The relationships are based on the flow rule, which defines the plastic strain increment in terms of the derivative with respect to stress of a plastic potential function. Because the yield function, Eq. (3-1), represents a generalization of stress versus deformation and strength versus deformation behaviors based on laboratory data, the function can be used to represent both the stress-deformation response and the effects of deformation on strength. Therefore, the plastic potential is assumed to be equivalent to the yield function, and the plastic strain increment is defined as follows based on plastic potential theory.

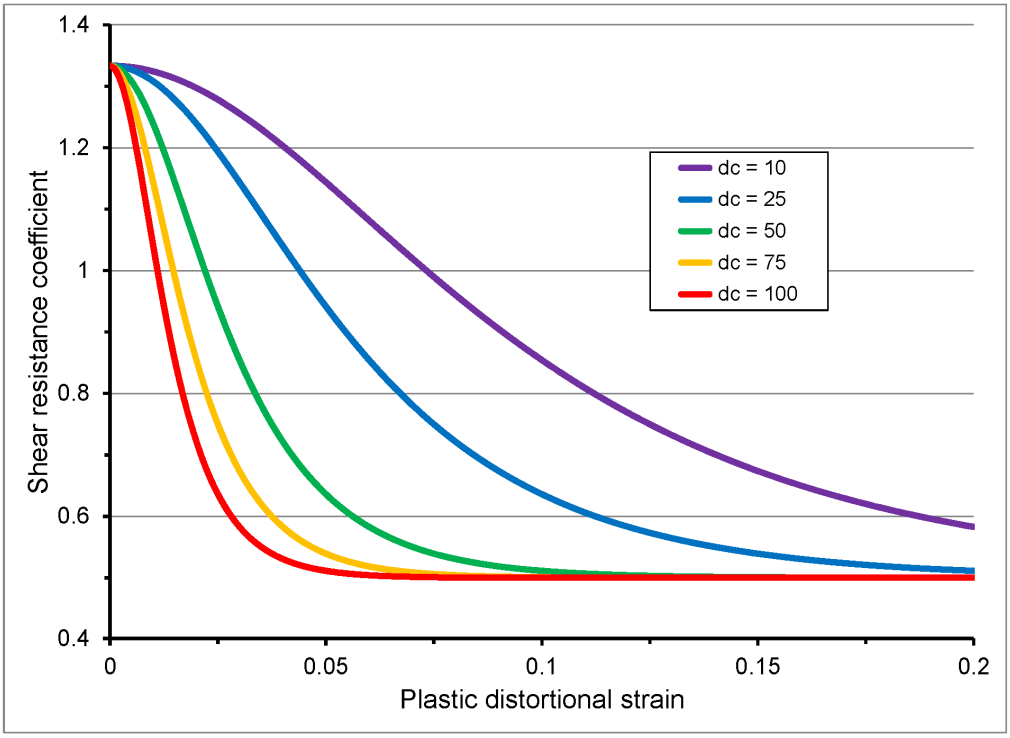

Figure 3-3. Shear Resistance Function $\mu(\Gamma^P)$ for $\mu_{\min} = 0.5$, $\mu_{\max} = 1.33$, and Selected Values of d_c

$$\Delta e_{ij}^{P} = \Lambda \frac{\partial F}{\partial \sigma_{ij}} \tag{3-8}$$

where Λ is a scalar factor that determines the absolute magnitude of plastic strain increment, whereas the derivative $\partial F/\partial \sigma_{ij}$ determines the relative magnitudes of the various components of plastic strain increment.

To evaluate Λ, we invoke the consistency condition, which defines a rule controlling potential stress change and material degradation due to plastic deformation. The consistency condition for salt rock is defined as follows based on the yield function.

$$\Delta F = \frac{\partial F}{\partial \sigma_{ij}} \Delta \sigma_{ij} + \frac{\partial F}{\partial a} \Delta a = 0 \tag{3-9}$$

where $a = b_1$ and b_2 is related to b_1 through Eq. (3-2). Therefore, the second term of Eq. (3-9) represents strength evolution due to plastic deformation. Equation (3-9) is central to the evaluation of plastic strain versus stress relationships. The various terms of the equation expand to the following.

$$\frac{\partial F}{\partial \sigma_{ij}} \ \left[\text{denoted } A_{ij}\right] = \frac{3S_{ij}}{2q} + \frac{1}{3a(1+kp)}\delta_{ij} \tag{3-10}$$

where $k = \partial b_2/\partial b_1$, S_{ij} is the deviatoric stress, and q is the deviatoric stress invariant (representing the distortional intensity of the stress tensor) as defined in Chapter 2 [Eqs (2-13) and (2-17)]. The stress increment $\Delta\sigma_{ij}$ is defined in Chapter 2 [Eq. (2-3)] in terms of its relationship with the strain increments, including plastic strain increment.

$$\frac{\partial F}{\partial a} = \frac{p}{a^2(1+kp)} \tag{3-11}$$

based on Eq. (3-1). Also,

$$\Delta a = -\frac{\Lambda\sqrt{3}}{2\mu^2}\left(\frac{\partial \mu}{\partial \Gamma^P}\right) \tag{3-12}$$

where $\mu(\Gamma^P)$, and thus $\partial\,\mu/\partial\Gamma^P$, is defined in Eq. (3-7). We substitute Eqs. (2-3), (3-10), (3-11), and (3-12) into the consistency condition [Eq. (3-8)] to obtain an expression for Λ, which we use in Eqs. (3-7) with (3-9) to evaluate the plastic strain increment. The resulting equations are as follows.

$$\Lambda = \frac{Q_{ij}\left(\Delta e_{ij} - \Delta e_{ij}^C\right)}{Q_D + \frac{p\sqrt{3}}{2(1+kp)}\left(\frac{\partial \mu}{\partial \Gamma^P}\right)} \tag{3-13}$$

where Q_{ij} and Q_D are given by the following equations:

$$Q_{ij} = \frac{\lambda\delta_{ij}}{a(1+kp)^2} + 2GA_{ij} \tag{3-14}$$

$$Q_D = A_{ij}Q_{ij} \tag{3-15}$$

and λ and G are described in Chapter 2 [Eq. (2-5)]. The plastic strain increment is then given by the following.

$$\Delta e_{ij}^P = \Lambda A_{ij} \tag{3-16}$$

3.3 Evolution of Elastic Stiffness Due to Plastic Deformation of Salt Rock

Section 3.1.2 describes a model for salt rock weakening (strength reduction) due to smoothing (roughness reduction) of shearing surfaces as a consequence of plastic deformation. Salt rock also could soften (i.e., experience reduction of elastic stiffness) if plastic deformation results in dilation of the particle skeleton. We describe a model in this section for dilation-dependent softening of salt rock.

Consider an element of the material that deforms from a resolved state with mean pressure p_0 and specific volume v_0 to a new state with mean pressure p and specific volume v. The specific volume increment Δv can be related to the change in mean pressure Δp as follows.

$$\varpi = \frac{\Delta v}{v_0} = -\kappa \frac{\Delta p}{p_a} \tag{3-17}$$

where $p_a = (p + p_0)/2$ is the average mean pressure, $\Delta p = p - p_0$, $\Delta v = v - v_0$, and κ is a strain-dependent compressibility parameter. Specific volume is the ratio of total volume to volume of solids, expressed as follows.

$$v = \frac{V}{V_s} = \frac{1}{1-\phi}; \qquad \phi = \frac{V_\mathrm{v}}{V} \tag{3-18}$$

where V is the total (skeleton) volume of an element consisting of a volume V_s of solid particles (minerals) and a volume V_v of pores (void space), such that $V = V_s + V_\mathrm{v}$ and the volume V is large enough to be a representative elementary volume, but small enough to be used as a basis for continuum description of the hydromechanical state. The parameter ϕ represents the porosity.

We assume that the solid (or mineral) particles are incompressible (i.e., a change in p alone does not cause any change in V_s). Therefore, the plastic volumetric strain increment $\Delta\varepsilon$ corresponding to an increment in specific volume from v_0 to v is given by the following.

$$\Delta\varepsilon = \frac{\Delta V_\mathrm{v}}{V_{\mathrm{v}0} + V_{s0}} = \frac{\Delta V_\mathrm{v}/V_s}{V_0/V_s} = \frac{\Delta v}{v_0} \tag{3-19}$$

Also, based on the definition of bulk modulus B_m as the pressure change per unit volumetric strain increment and using Eqs. (3-17) and (3-19), we obtain the following.

$$B_m = -\frac{\Delta p}{\Delta\varepsilon} = \frac{p_a}{\kappa} \tag{3-20}$$

During plastic deformation, changes in p could be small or insignificant, such that a change in B_m due to a change in κ is more important than any contribution due to change in p_a. Therefore, to model the effect of dilation on B_m we evaluate the effects of κ with p_a held constant. For this condition, Eq. (3-20) can be re-written as follows.

$$B_m = \left(\frac{\kappa_\mathrm{min}}{\kappa}\right)^{\mathrm{init}} B_m \tag{3-21}$$

where ${}^{\mathrm{init}}B_m$ and κ_min are the initial (zero-strain) state values of B_m and κ, respectively.

During plastic deformation, κ increases monotonically as dilation increases and can be modeled using the following relationship.

$$\kappa = \kappa_\mathrm{max} - \frac{2(\kappa_\mathrm{max} - \kappa_\mathrm{min})}{\exp[d_k(v/v_\mathrm{min} - 1)] + \exp[-d_k(v/v_\mathrm{min} - 1)]} \tag{3-22}$$

where κ_max is a maximum value that κ approaches asymptotically as specific volume increases due to dilation, d_k is a "decay" parameter that controls the rate of change of κ with respect to v, and v_min is the value of v at the zero-strain (initial) state.

Note that, as defined in connection with Eq. (3-17), v_0 is the value of v at the beginning of a state increment that includes plastic deformation. Values of v and v_0 are related as follows.

$$v = v_0\left(1 + \frac{\Delta v}{v_0}\right) = v_0(1 + \Delta\varepsilon^P) \tag{3-23}$$

where $\Delta\varepsilon^P$ is the plastic volumetric strain increment. If other deformation mechanisms contribute to dilation, then their contribution during the increment should be added to $\Delta\varepsilon^P$.

Examples of κ-v and B_m-v relationships (for three d_k values) based on a prescribed sequence of ε^P values are shown in Figures 3-4 and 3-5. As the figures show, the stiffness reduction due to plastic deformation model is sensitive to the parameter d_k. Because the value of this parameter will likely not be available from any measurement, sensitivity analyses may be needed to choose values for modeling.

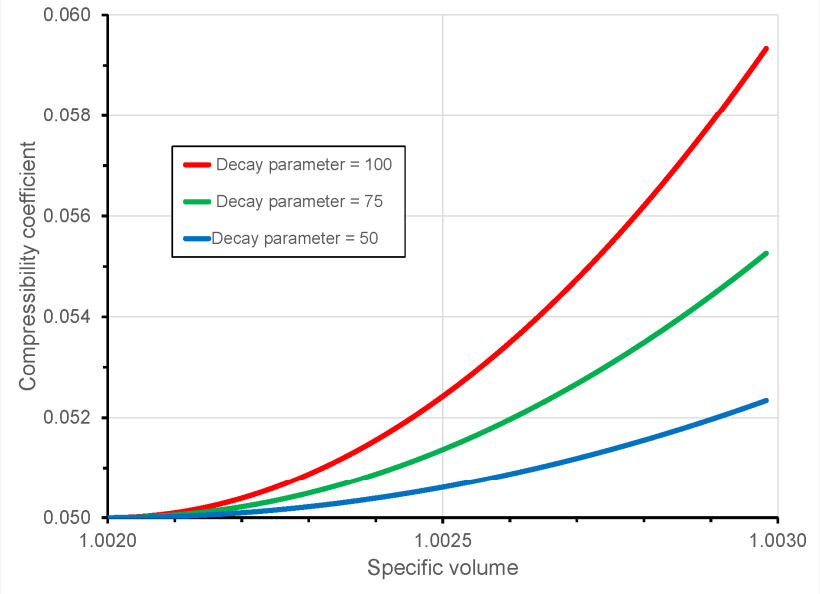

Figure 3-4. Example κ-v Relationships (for Three d_k Values) Based on a Prescribed Sequence of ε^P Values With $v_{\min} = 1.002$

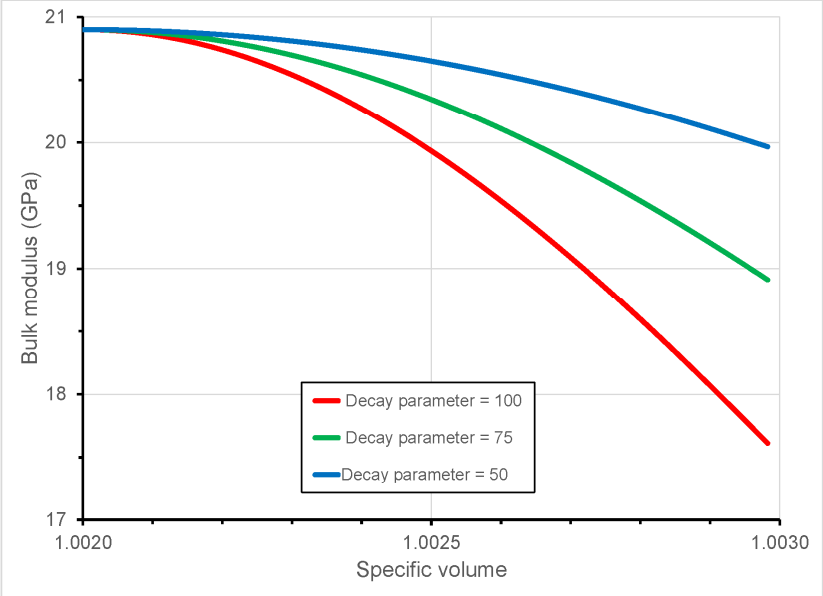

Figure 3-5. Example B_m-v Relationships (for Three d_k Values) Based on a Prescribed Sequence of ε^P Values With $v_{\min} = 1.002$

4 NUMERICAL MODELING OF PREVIOUS IN SITU TESTS CONDUCTED AT THE WASTE ISOLATION PILOT PLANT (WIPP)

The constitutive model described in Chapters 2 and 3 was used with the geomechanical computer code FLAC (Itasca Consulting Group, 2016) to model in-situ experiments conducted previously at the WIPP. The WIPP experiments consisted of long term measurements of rock convergence around two underground openings constructed in bedded salt—test facility Rooms B and D—as described in Rath and Argüello (2012). Room D remained at ambient temperature conditions, while Room B was subjected to applied thermal loads using embedded heaters below the floor. The cross sectional areas of the rooms are 5.5 m [16.4 ft] wide and 5.5 m [16.4 ft] high, located at a depth of 646 m [2,119 ft] below the ground surface. The subsurface stratigraphy at the location of the rooms, as shown in Rath and Argüello (2012, Figure 3-1), consists mainly of layers of halite and argillaceous halite interrupted by several horizontal clay seams.

The numerical modeling was focused on Room B, the heated underground opening. However, because the two rooms have identical geometry and essentially identical geology, several analysis cases of Room D (nonheated room) were performed to determine an appropriate material model for Room B analysis.

4.1 Model Geometry and Initial and Boundary Conditions

Site specific data and loading conditions used in the model and the field measurement data used for comparison with model results were obtained from Rath and Argüello (2012). Two-dimensional (2-D) plane strain models were developed using FLAC at the mid-section of the rooms. The test section of unheated Room D is in the middle 74.4 m [244.0 ft] of the 93.3 m [306.0 ft] long room. The heated Room B has heaters placed below the floor, symmetric with the center line of the room. The heaters, which simulate the effects of heat-generating radioactive waste canisters, were placed at regular intervals in bore holes in the middle 24.4 m [80.0 ft] of the 93.3 m [306.0 ft] long room. More heaters were placed at either end of the room to provide a uniform temperature distribution along the entire length of the test section. Because of these symmetries, 2-D models are appropriate for studying the thermal and mechanical responses of the room in the experiments.

The model geometry based on Rath and Argüello (2012) is shown in Figure 4-1(a). Half of the room section was modeled using a vertical plane of symmetry along the center line of the room. The top and bottom boundary pressure is in accordance with overburden pressure (Rath and Argüello, 2012). The initial vertical stress (σ_v) varies linearly with depth and the initial horizontal stress (σ_h) was set to 1.5 times the vertical stress based on previous studies in Ofoegbu and Dasgupta (2016). For boundary conditions on vertical boundaries, displacement in the horizontal direction is restrained. The excavation boundary is, however, traction-free.

The thermal boundary condition is shown in Figure 4-1(b). The initial temperature of the model is 300 K [26.9 °C, 80.3 °F] and the model boundaries are held at the initial temperature through the simulation period. The heater is placed along the plane of symmetry. The heater location and length are shown in Figure 4-1(b), based on Rath and Argüello (2012). The thermal load was varied with time as described in Ofoegbu and Dasgupta (2016).

The modeling sequences used for Rooms B and D are similar to those described in Ofoegbu and Dasgupta (2016). For unheated room D, a static stress field was developed using initial

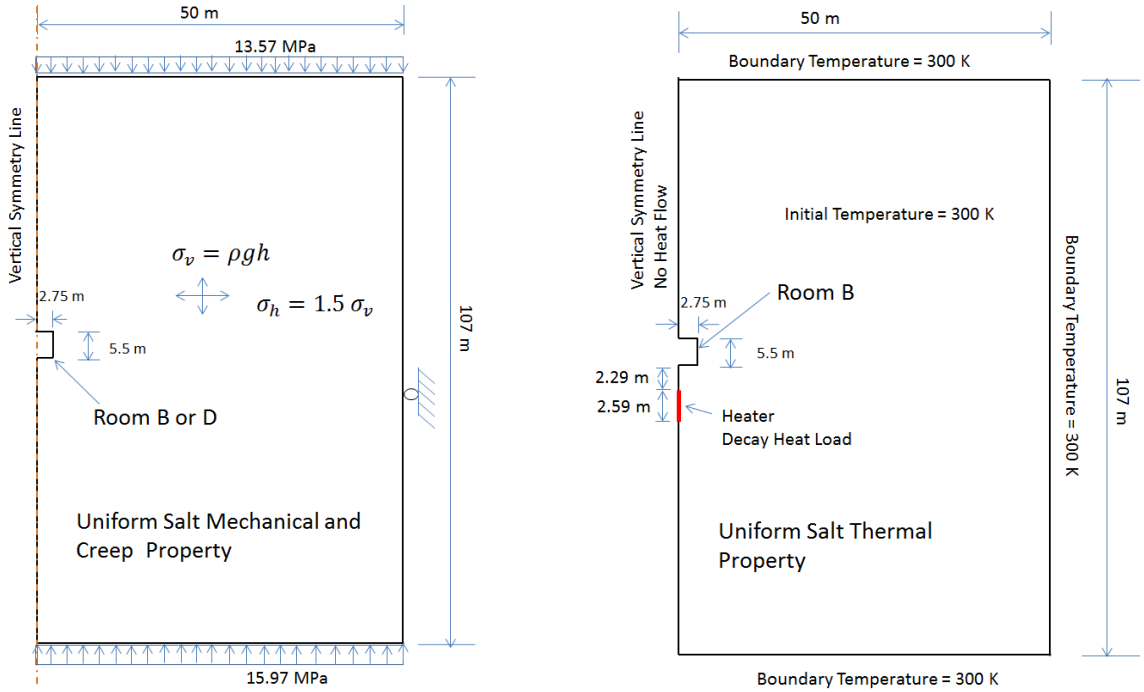

Figure 4-1. Model Geometry and Boundary Conditions for (a) Mechanical and (b) Thermal Models [1.0 MPa = 145.03 psi, 1.0 m = (3.28 ft)]

stress conditions. In the model, creep was simulated for 1,000 days after excavation of Room D. The ambient temperature for Room D, which remained constant throughout the analysis, was assumed to be 300 K.

For the heated Room B simulation, one-way coupling of thermal and mechanical responses was employed as described in Ofoegbu and Dasgupta (2016). A thermal analysis was first performed using FLAC to generate the temperature of the model discretized zones for the heat load applied at the heater location for 1,000 days. The computed temperature was saved at specific intervals during the thermal simulation for application in the mechanical model. The thermal analysis discussed in Ofoegbu and Dasgupta (2016) was used in the mechanical calculations. The mechanical model was initiated in a similar way as for the Room D model; however, creep analysis at the ambient temperature of 300 K was performed for 324 days. The zone temperature data were provided as inputs into the mechanical model at specific times to ensure the creep and thermal times were synchronized.

The Room D model with clay layers is shown in Figure 4-2. Clay layers D to L closer to the excavated area were incorporated in the model based on the stratigraphy obtained from Rath and Argüello (2012). The clay seams noted in Rath and Argüello (2012) are primarily local "horizontal concentrations of disseminated clay stringers." Therefore, the seams can be incorporated in the models as contact surfaces with prescribed clay properties (Rath and Argüello, 2012). Interfaces between grids can be modeled explicitly in FLAC. These interfaces are planes upon which slip and/or separation is allowed. Interfaces are characterized by Coulomb sliding and/or tensile separation. Interfaces have the properties of friction, cohesion, dilation, normal and shear stiffness, and tensile strength.

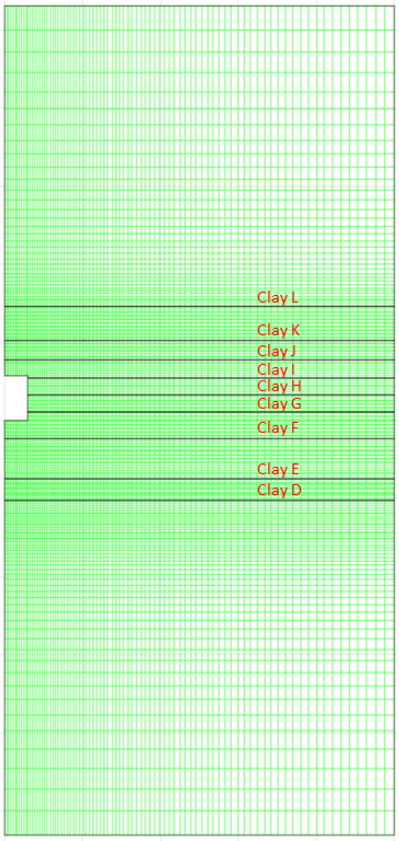

Figure 4-2. FLAC Model Geometry of Room D and the Clay Layers

4.2 Material Model Options

Several material model options were established based on the material modeling approach described in Chapters 2 and 3. The parameter values in those model options are described in this section and were used in different analysis cases as described in Section 4.3.

4.2.1 Linear Elastic Parameters

The linear elastic parameter values for halite used in the modeling are similar to the values in Table 4-1 of Ofoegbu and Dasgupta (2016) and are given as follows:

Young's modulus $E = 6.27 \times 10^3$ MPa
Poisson's ratio $\nu = 0.45$

4.2.2 Nonlinear Elastic Parameters

The nonlinear elastic model based on dilation-dependent bulk modulus is described in Section 3.3. The parameters and the values assumed are given as follows:

Elastic (or initial) bulk modulus $K_E = 2.09 \times 10^4$ MPa
Minimum compressibility coefficient $\kappa_{\min} = 0.05$
Maximum compressibility coefficient $\kappa_{\max} = 2.0$
Decay parameter for compressibility coefficient $d_k = 100$
Minimum (i.e., initial) specific volume $\upsilon_{\min} = 1.002$

4.2.3 Creep Parameters

The parameters used for the creep model in Table 4-1 of Ofoegbu and Dasgupta (2016) are used in this analysis. Note that the dilatant creep coefficients and the exponent were not used, because the material deformation due to material damage is modeled using the plasticity model discussed in Chapter 3. The transient creep parameters are listed in the following subsections.

4.2.3.1 Constant Transient Creep Parameters

Three cases of constant transient creep parameters were studied.

(a) $a_0 = 0.008$ $a_1 = 1{,}250$, and $a_2 = 0.30$.
(b) $a_0 = 0.008$ $a_1 = 1{,}250$, and $a_2 = 0.375$.
(c) $a_0 = 0.008$ $a_1 = 1{,}500$, and $a_2 = 0.375$.

4.2.3.2 Variable Transient Creep Parameters

(a) Creep model with $a_0 = a_0(R_s)$ [modeled using Ofoegbu and Dasgupta (2016, Equation 3-2) with $b_1 = 100$ and $b_2 = 50$]

(b) Creep model with transient creep parameter a_0, defined as a function of the stress invariants ratio $R_s = q/p$ to represent the effects of small deviatoric stress on creep strain rate (Section 2.1). The parameter values are:

$a_{00} = 0.1$ Value of a_0 for $R_s = 0$

$a_{01} = 0.004$ Value of a_0 at $R_s = R_{s1}$

$a_{02} = 0.01$ Value of a_0 at $R_s = R_{s2}$

$R_{s1} = 0.5$ Value of R_s at which the models for small deviatoric stress and larger deviatoric stress give the same value for a_0

$R_{s2} = 6.0$ Value of R_s at an arbitrary point on the larger deviatoric stress model

$c_2 = 1.5$ Fitting parameter for small deviatoric stress model

$b_1 = 100$ Fitting parameter for larger deviatoric stress model

4.2.4 Plasticity Model Parameters

The plasticity model described in Chapter 3 requires five parameters. Following are the parameters and values used in all model cases where plasticity is used.

Cohesive strength parameter, $q_0 = 10$ MPa
Yield function parameters, $k_0 = 0.0$, $k_1 = 0.024$
Maximum shear resistance coefficient, $\mu_{\max} = 2.0$
Minimum shear resistance coefficient, $\mu_{\min} = 0.1$
Shear resistance decay coefficient, $d_c = 10$

4.2.5 Clay Seam Parameters

Clay seams are represented as relatively weak interfaces between layers of salt rock. The interface properties required in the model and the parameter values are:

Friction angle = $20°$
Cohesion = 0.02 MPa
Tensile strength = 0.001 MPa
Normal stiffness = 10^6 MPa/m
Shear stiffness = 5×10^4 MPa/m

4.2.6 Thermal Parameters

The thermal parameters used in the Room B analysis are defined in Table 4-1 of Ofoegbu and Dasgupta (2016).

Thermal expansivity, $\alpha = 4.2 \times 10^{-5}\ 1/K$
Thermal conductivity, $\lambda = \lambda_{300}(300/T)^{\gamma}$
where $\lambda_{300} = 4.32 \times 10^5\ (J/(m.day.K))$, $\gamma = 1.14$, and T is absolute temperature in Kelvin (K).

4.3 Analysis Cases for WIPP Rooms

Analysis Cases 1-7 are associated with modeling convergence of unheated Room D and Case 8 relates to Room B. As discussed previously, Rooms B and D in the WIPP experiments differ only in that a thermal load was applied in Room B, whereas Room D was held at ambient temperature. Therefore, several analysis cases of Room D were performed to choose a material model combination for Room B. The analysis cases are summarized in Table 4-1 and described in more detail in this section.

4.3.1 Analysis Case 1: Linear Elasticity and Creep

This analysis was performed previously (Section 4.2 of Ofoegbu and Dasgupta, 2016) and was not repeated for this report. As Ofoegbu and Dasgupta (2016) discussed, the results showed that this material model combination is not adequate to represent inelastic deformations around the test excavations. The calculated convergence reached a maximum of 120 mm [4.7 in] (vertical convergence) and 63 mm [2.5 in] (horizontal convergence) and stabilized after approximately 300 days. In contrast, the measured convergence gradually increased, reaching approximately 300 mm [11.8 in] (vertically) and 220 mm [8.7 in] (horizontally) at 1,500 days, and continued increasing after 1,500 days.

4.3.2 Analysis Cases 2 and 3: Nonlinear Elasticity, Creep, and Plasticity

This analysis case used nonlinear elasticity, creep, and plasticity models. Elastic deformation was represented using the nonlinear elastic model (Section 1.1.2), creep was represented using constant parameters (Section 1.1.3.1), and the plasticity model (Section 1.1.4) was introduced to account for instantaneous inelastic deformation that is beyond the scope of creep modeling. Such inelastic deformation includes inter-particle movements driven by mechanisms that are similar to creep but occur instantaneously, could progress to observable material failure, and are controlled by stress and material deformation history.

Table 4-1. Description of Analysis Cases		
	Analysis Case	**Brief Description of Material Model**
Case 1	Room D: Case 1 (2016)	Linear elastic model; Creep model with constant a_0
Case 2	Room D: Model with coupled creep and plasticity with nonlinear elasticity	Nonlinear elastic model Plasticity model Creep model —variable transient creep parameter $a_0 = a_0(R_s)$; modeled using Ofoegbu and Dasgupta (2016, Equation 3-2) with $b_1 = 100$ and $b_2 = 50$
Case 3	Room D: Creep model with constant parameters $a_0 = 0.008$, $a_1 = 1250$; $a_2 = 0.30$;	Nonlinear elastic model Plasticity model Creep model —transient creep parameters constant
Case 4	Room D: Same as Case 2 except a revised $a_0(R_s)$ function is used to address effects of creep under small deviatoric stress.	Nonlinear elastic model Plasticity model Creep model —variable transient creep parameter $a_0 = a_0(R_s)$; a_1 and a_2 are constant
Case 5	Room D: Clay seams represented as interface between salt layers.	Nonlinear elastic model Plasticity model Creep model —constant transient creep parameters (same as Case 3)
Case 6	Room D: Creep model with constant parameters $a_0 = 0.008$, $a_1 = 1250$; $a_2 = 0.375$;	Nonlinear elastic model Plasticity model Creep model with constant —constant transient creep parameters
Case 7	Room D: Creep model with constant parameters $a_0 = 0.008$, $a_1 = 1{,}500$; $a_2 = 0.375$;	Nonlinear elastic model Plasticity model Creep model with constant —constant transient creep parameters
Case 8	Room B (heated): analysis described in Section 4.4; Creep model with constant parameters $a_0 = 0.008$, $a_1 = 1{,}250$; $a_2 = 0.30$	Nonlinear elastic model Plasticity model Creep model with constant —constant transient creep parameters (same as Case 3)

Analysis Cases 2 and 3 differ in their representations of transient creep parameter a_0. In Analysis Case 2, a_0 is represented as a function of q/p as described in Ofoegbu and Dasgupta (2016), whereas $a_0 = 0.008$ in Analysis Case 3.

The calculated convergence histories (Figures 4-3 and 4-4) show that the plasticity model option is a desirable contribution to the material modeling. The shape of the calculated convergence history is similar to the shape of the measured history. The calculated convergence at 1,300 days is within 75–80 percent of the measured convergence. Three aspects of this material model combination could be further improved:

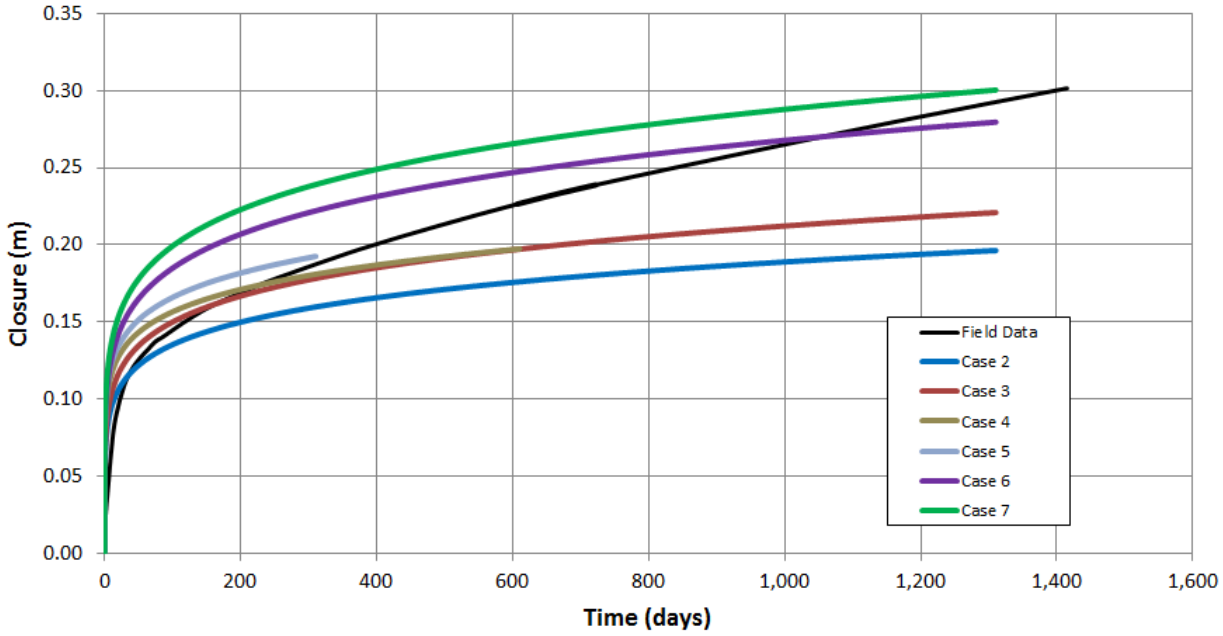

Figure 4-3. Calculated Vertical Convergence of Room D (Ambient Temperature Test) From Several Analysis Cases Compared With the In-Situ Measurement

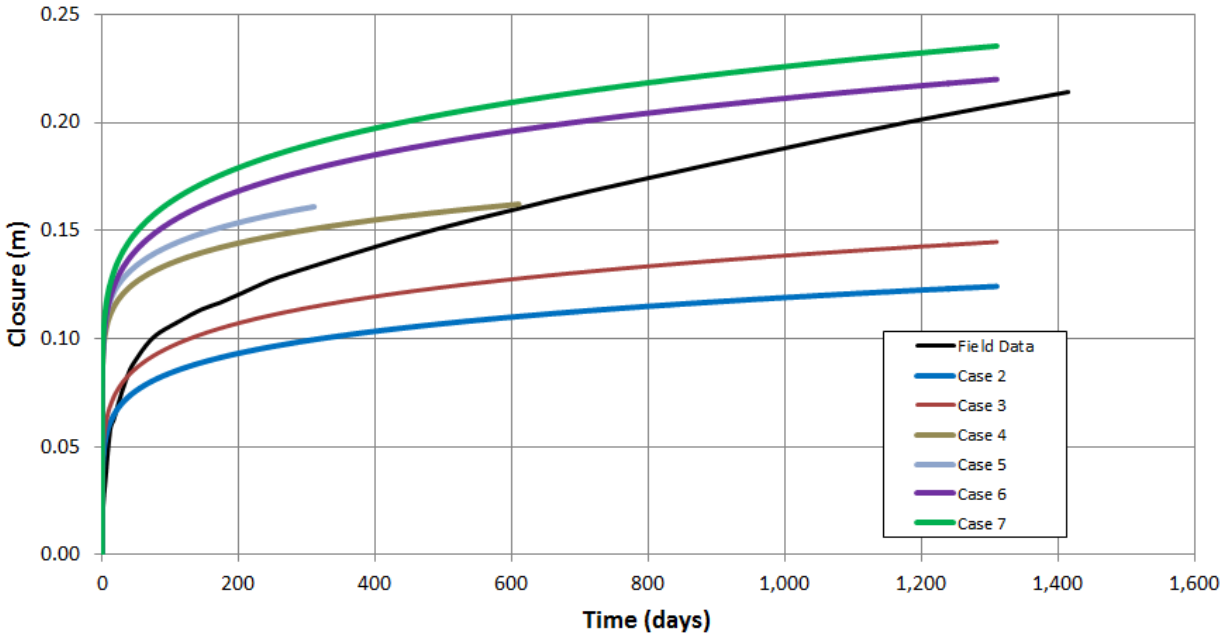

Figure 4-4. Calculated Horizontal Convergence of Room D (Ambient Temperature Test) From Several Analysis Cases Compared With the In-Situ Measurement

1. Values of the three transient creep parameters a_0, a_1, and a_2.
2. Values of plastic model parameters.
3. Coupling of plastic and creep strains. Currently, creep and plastic strain increments are coupled through deviatoric stress. Coupling through strain (distortional strain, dilation, or both, potentially through a_0) could be stronger but needs to be investigated further.

4.3.3 Analysis Case 4: Nonlinear Elasticity, Creep (With Modified a_0 Function), and Plasticity

This analysis case is the same as Case 2 except a revised $a_0(R_s)$ function was applied to explore using this approach to address the effects of creep under small deviatoric stress. As the results show (Figures 4-3 and 4-4), although the approach resulted in increased creep under small deviatoric stress, the effect on horizontal convergence appears excessive. The authors did not use the $a_0(R_s)$ function for further analysis.

4.3.4 Analysis Case 5: Clays Seams Included as Interfaces

In this analysis case, salt rock is represented as layers with material properties as described for Analysis Case 3. Additionally, the layer interfaces were modeled as weak relative to the layers to represent clay seams. The interface properties are as described in Section 4.2.6. The mechanical effects on the convergence are sensitive to both stiffness and strength properties of the layer. Since these properties are not directly measurable in the laboratory, they are assumed based on available information in the literature and further calibrated based on the expected mechanical response. Preliminary analyses were performed to test the model behavior. In one case, the interface properties were assumed to have strength to inhibit slip or opening. The model responded like a continuum rock mass, as expected, and the convergence profile is similar to Case 3. In the other case, the layer properties were assumed to be very weak and the model showed very high convergence compared to the field measurements, primarily caused by opening (increased aperture) of the interfaces on the roof. These two extreme cases showed that the modeling approach is reasonable. Further model runs are continuing with appropriate combinations of the interface properties.

4.3.5 Analysis Cases 6 and 7: Nonlinear Elasticity, Creep (With Modified Parameter Values), and Plasticity

These analysis cases are the same as Case 3, except that the creep parameter values were modified to examine their effects on calculated convergence. In these cases, the transient creep parameters are the following constant values:

Case 3: $a_0 = 0.008$, $a_1 = 1{,}250$, and $a_2 = 0.30$
Case 6: $a_0 = 0.008$, $a_1 = 1{,}250$, and $a_2 = 0.375$
Case 7: $a_0 = 0.008$, $a_1 = 1{,}500$, and $a_2 = 0.375$

The convergences for Cases 6 and 7 are compared with the measured convergence and with Case 3. In Figure 4-3, both Cases 6 and 7 predict vertical convergence higher than the measured values up to about 800 days; thereafter, the calculated convergences are comparable to the measured data. In Figure 4-4, the horizontal convergence for both Cases 6 and 7 is higher than the measured values through the measurement period; however, the models appear to be trending toward the measured data at later times.

4.4 Analysis Case 8 for Room B Heated Experiment

The material model combination for Analysis Case 3 was used to conduct an analysis of the heated Room B experiment. Case 3 resulted in vertical and horizontal convergences that are closest to the in-situ measurements in unheated Room D. The material model combination consisted of nonlinear elasticity, plasticity, and creep (with $a_0 = 0.008$, $a_1 = 1{,}250$, and $a_2 = 0.30$). The calculated vertical and horizontal convergences for the heated conditions are compared with the measured convergence from the Room B in Figure 4-5. The convergence history shows an increase in convergence at the start of thermal loading, consistent with the measured convergence history. However, the calculated magnitude of convergence is smaller than the measured magnitude.

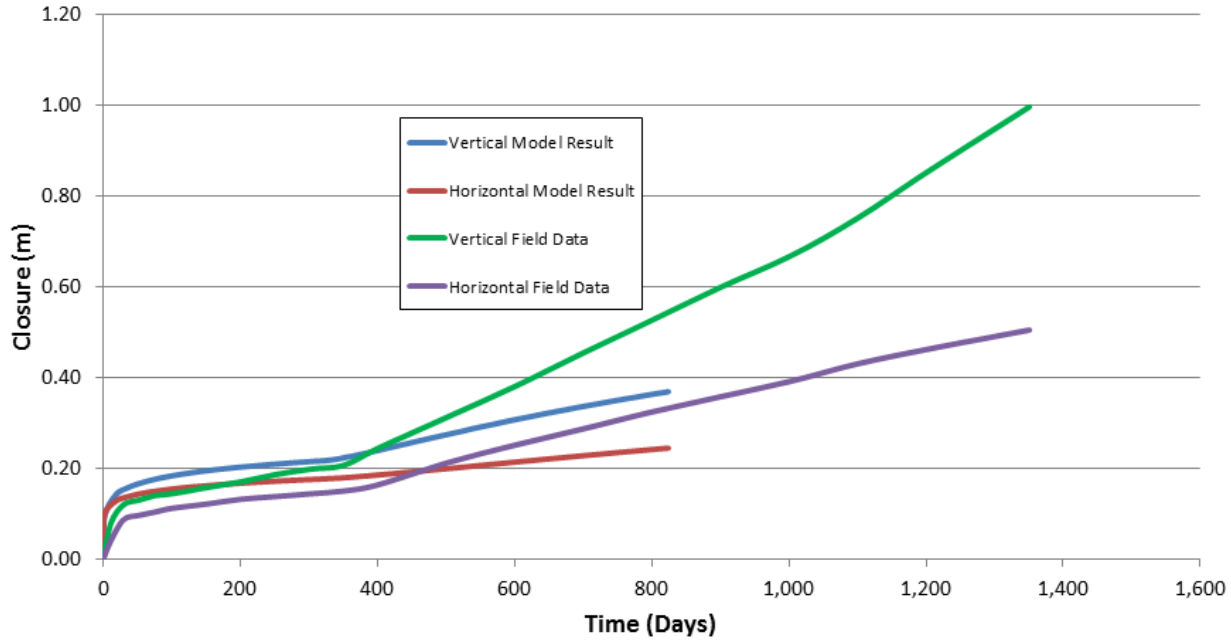

Figure 4-5. Calculated Vertical and Horizontal Convergence of Room B (Heated Experiment) Compared With the In-Situ Measurement (Case 8)

5 CONCLUSIONS

This report describes numerical simulations of in situ experiments at the WIPP site using an updated constitutive model. The simulations were performed to evaluate approaches to modeling salt rock mechanical behavior in underground openings. Simulations were performed for ambient conditions (Room D) to evaluate approaches to material modeling and for heated conditions (Room B) to evaluate thermal effects. Model results for Room D are applicable to Room B because the rooms have the same geometry and closely similar geologic conditions. Material models based on creep and coupled creep and plasticity were evaluated.

5.1 Coupled Creep and Plasticity Model

Models based on coupled creep and plasticity resulted in improvements in the calculated convergence relative to the creep-only model. Compared to Ofoegbu and Dasgupta (2016), the model showed improvements in the shape of the calculated convergence history and the magnitude of calculated convergence improved to approximately 75 percent of the measured convergence approximately 1,200 days after excavation. Based on these results, coupled creep and plasticity modeling likely will lead to better understanding of the time-dependent mechanical behavior of salt rock surrounding heated underground openings. This modeling approach can be improved, as described subsequently.

5.2 Creep Contribution from Small Deviatoric Stress Conditions

The authors investigated contributions to convergence due to rock creep from small deviatoric stress conditions. The investigation was based on describing the transient creep parameter a_0 as a function of deviatoric stress, represented through a nondimensional stress ratio q/p. Although increased creep rates from small deviatoric stress conditions resulted in increased convergence, the shape of the calculated convergence history departed from the shape of the measured history enough to indicate that the calculated effect is not consistent with rock behavior around the openings.

5.3 Effect of Clay Seams

Deformation of clay seams or clayey interfaces between salt rock layers could contribute to overall rock behavior around the openings. One approach to account for deformation of clay seams was evaluated by explicitly representing the seams as contact surfaces using the interface feature in FLAC. Although this is a potential improvement, interface parameters of the clay seams need to be calibrated in order to obtain the measured convergence. In this approach, potential creep in the clay seams is not included. The contribution of the clay seams can be accounted for implicitly as a thin clay zone instead of an interface and a material model based on coupled creep and plasticity can be applied.

5.4 Thermal Effects

The calculated convergence history for Room B shows an increase in convergence at the start of thermal loading, consistent with the measured convergence history. However, the calculated magnitude of convergence is smaller than the measured magnitude. The authors expect that the accuracy of the calculation can be improved, as discussed in Section 5.5.

5.5 Material Model Modifications to Improve Accuracy of Calculated Behavior

The model results led to identification of potential modifications in material modeling that may lead to better understanding of salt rock behavior around heated openings. The modifications described in the following subsections should improve the coupling of creep and plastic deformation modeling and thermal-mechanical coupling.

5.5.1 Coupling of Creep and Plastic Deformations

In the material model used for the simulations, creep and plastic deformations are coupled, somewhat weakly, through deviatoric stress. Creep rates are proportional to a power function of deviatoric stress, while plastic deformations are driven by deviatoric stress. Both plastic and creep deformations cause the deviatoric stress to decrease. The coupling, which is dependent on a decrease in deviatoric stress, appears to be weak.

The strength of coupling of the two deformation mechanisms could be increased by representing some of the controlling parameters as functions of distortional strain. Both creep and plastic deformations contribute to distortional strain, at times in comparable magnitudes, such that properties dependent on distortional strain will be affected by each deformation mechanism. The effect will provide a feedback mechanism to increase or decrease the deformation rates.

5.5.2 Thermal and Mechanical Coupling

Thermal changes affect mechanical deformation through increased stress due to suppressed thermal expansion. The mechanical effects of thermal loading depend on the temperature and property gradients, mechanical boundary conditions, and thermal expansivity. These effects are well understood and are represented in the thermal modeling. However, additional thermal effects could result from thermal strain affecting mechanical behavior, such as through dilation-dependent bulk modulus or other parameters dependent on distortional strain. The approach to representing the effects of thermal strain on mechanical property needs additional investigation, because thermal effects on dilation and distortional strain are not defined explicitly.

6 REFERENCES

Desai, C.S. and H.J. Siriwardane. *Constitutive Laws for Engineering Materials with Emphasis on Geologic Materials*. Englewood Cliffs, New Jersey: Prentice-Hall, Inc. 1984.

European Commission. "Compilation of Existing Constitutive Models and Experimental Field or Laboratory Data for the Thermal-Hydraulic (THM) Modelling of the Excavation Disturbed Zone (EDZ) in Rock Slat." Sixth Framework Programme. EURATOM Radioactive Waste Management. THERESA Project. Work Package 3 Deliverable 5. 2007.

Hunsche U. and A. Hampel. "Rock Salt—the Mechanical Properties of the Host Rock Material for a Radioactive Waste Repository." *Engineering Geology*. Vol. 52. pp. 271–291. 1999.

Itasca Consulting Group, Inc. "FLAC Fast Lagrangian Analysis of Continua." Version 8. Minneapolis, Minnesota: Itasca Consulting Group, Inc. 2016.

_____. "FLAC Fast Lagrangian Analysis of Continua." Version 7. Minneapolis, Minnesota: Itasca Consulting Group, Inc. 2011.

Mellegard, K.D. and D.E. Munson. "Laboratory Creep and Mechanical Tests on Salt Data Report (1975–1996) Waste Isolation Pilot Plant (WIPP) Thermal/Structural Interaction." SANDIA REPORT, SAND96-2765. Albuquerque, New Mexico: Sandia National Laboratories. 1997.

Ofoegbu, G. and B. Dasgupta. "Implementation of a Creep Model in FLAC to Study the Thermomechanical Response of Salt as a Host Repository Medium—Progress Report." San Antonio, Texas: Center for Nuclear Waste Regulatory Analyses. 2016.

Rath, J.C. and J.G. Argüello. "Revisiting Historic Numerical Analyses of the Waste Isolation Pilot Plant (WIPP) Room B and D *In-Situ* Experiments Regarding Thermal and Structural Response." SANDIA REPORT, SAND20–12–7525. Albuquerque, New Mexico: Sandia National Laboratories. 2012.

Reedlunn, B. "Reinvestigation Into Closure Predictions of Room D at the Waste Isolation Pilot Plant." SAND2016-9961. Albuquerque, New Mexico: Sandia National Laboratories. 2016.